による定位的放射線治療でも良好な治療成績をあげており，ⅠB期（T2N0M0）については局所再発や原発巣のみを標的とする現在の方法では領域リンパ節再発も生じているので，更なる工夫が必要である。しかしながら，手術不適応・手術拒否患者においては陽子線・重イオン線治療は，治療の選択肢のひとつとしてその役割が十分あるものと思われる。また，今後は局所進行肺癌で標準となっている化学放射線療法において陽子線治療を併用した線量増量あるいは副作用低減の意義を検討するべきであろうと思われる。

ちなみに，国内で荷電重粒子線治療を実施しているのは国立がんセンター東病院（陽子線），筑波大学陽子線医学利用研究センター（陽子線），兵庫県立粒子線医療センター（陽子線・炭素イオン線），放射線医学総合研究所（炭素イオン線），若狭湾エネルギー研究センター（陽子線），静岡がんセンター（陽子線）の6施設のみである。また，国立がんセンター東病院では2001年7月に国から「高度先進医療」の適用を受け，費用は患者自己負担（国立がんセンター東病院の場合，一連で2,883,000円）として実施しており，他の施設も金額的にはほぼ同様な状況である。施設の普及

と保険収載が望まれるところである。

参 考 文 献

1) 辻比呂志, 辻井博彦, 奥村敏之ほか: 筑波大学における陽子線治療の初期治療成績. 日放腫会誌, 7: 303-313, 1995.
2) Shioyama, Y., Tokuuye, K., Okumura, T. et al.: Clinical evaluation of proton radiotherapy for non-small-cell lung cancer. Int J Radiat Oncol Biol Phys, 56: 7-13, 2003.
3) Slater, J. M., Archambeau, J. O., Miller, D. W. et al.: The proton treatment center at Loma Linda University Medical Center: Rationale and description of its development. Int J Radiat Oncol Biol Phys, 22: 383-389, 1991.
4) Bush, D. A., Slater, J. D., Bonnet, R. et al.: Proton-beam radiotherapy for early-stage lung cancer. Chest, 116: 1313-1319, 1999.
5) Bush, D. A., Slater, J. D., Shin, B. B. et al.: Hypofractionated proton beam radiotherapy for stage I lung cancer. Chest, 126: 1198-1203, 2004.
6) 荻野尚: 国立がんセンターにおける陽子線治療の計画. Biotherapy, 13: 266-268, 1999.
7) 二瓶圭二, 石倉聡, 荻野尚ほか: 非小細胞肺癌に対する陽子線治療の臨床第Ⅰ相試験. 日放腫会誌, 13(Suppl 1): 90, 2001.
8) Nihei, K., Ogino, T., Ishikura, S. et al.: Proton therapy for stage I non-small cell lung cancer(NSCLC). Int J Radiat Oncol Biol Phys, 60(suppl): 282, 2004.
9) Miyamoto, T., Yamamoto, N., Nishimura, H. et al.: Carbon ion radiotherapy for stage I non-small cell lung cancer. Radiother Oncol, 66: 127-140, 2003.

Distributions of β^+ decayed nuclei generated in the CH$_2$ and H$_2$O targets by the target nuclear fragment reaction using therapeutic MONO and SOBP proton beam

Teiji Nishio,[a] Takashi Sato, Hideaki Kitamura, and Koji Murakami
Department of Radiology, National Cancer Center, Kashiwa, 6-5-1 Kashiwano-ha, Kashiwa-shi, Chiba 277-8577, Japan

Takashi Ogino
Department of Proton Radiology, National Cancer Center, Kashiwa, 6-5-1 Kashiwano-ha, Kashiwa-shi, Chiba 277-8577, Japan

In proton radiotherapy, the irradiation dose can be concentrated on a tumor. To use this radiotherapy efficiently in the clinical field, it is necessary to evaluate the proton-irradiated area and condition. The proton-irradiated area can be confirmed by coincidence detection of pair annihilation gamma rays from β^+ decayed nuclei generated by target nuclear fragment reaction of irradiated proton nuclei and nuclei in the irradiation target. In this study, we performed experiments of proton irradiation to a polyethylene (PE:CH$_2$) target containing ^{12}C nuclei, which is a major component of the human body, and a gelatinous water (H$_2$O) target containing ^{16}O nuclei at different proton irradiation energy levels under different beam conditions of mono-energetic Bragg peak and spread-out Bragg peak. The distribution of the activity in the target after proton irradiation was measured by a positron emission tomography (PET) apparatus, and compared with the calculated distribution. The temporal dependence of the activity distribution during the period between the completion of proton irradiation and the start of measurement by the PET apparatus was examined. The activity by clinical proton irradiation was 3 kB/cc in the PE target and 13 kB/cc in the water target, indicating that the intensity was sufficient for the evaluation of the distribution. The range of the activity distribution against the physical range was short (several millimeter water equivalent length), indicating the presence of target dependence. The range difference in the water target was slightly large with time dependence until the start of measurement. The difference of the lateral widths with full width half at maximum in the distributions of the measured irradiated dose and activity was within 1 mm. © *2005 American Association of Physicists in Medicine.*
[DOI: 10.1118/1.1879692]

I. INTRODUCTION

Recently, use of heavy charged particle radiotherapy has been spreading throughout the world, and in Japan, proton radiotherapy has been performed at the National Cancer Center (Kashiwa), Tsukuba University, Wakasawan Energy Research Center, and Shizuoka Cancer Center, carbon radiotherapy at the National Institute of Radiological Sciences, and proton and carbon radiotherapy at Hyogo Ion Beam Medical Center.[1] In heavy charged particle radiotherapy, targets in patients can be irradiated by a charged particle beam, but without accurate control, the beam may miss the targets. To take advantage of heavy charged particle beams, it is very important to directly evaluate the irradiated area and condition in patients.

Radioactive ion beam generation technologies have been developed in the past dozen or so years, and used for basic physical studies.[2] Medical application of the beam was first performed by LBL (Lawrence Berkeley Laboratory) in the USA,[3] and the application of the beam is currently being studied at the National Institute of Radiological Sciences.[4,5] Incident radioactive ion beams of β^+ decayed nucleus (positron-emitting nucleus) stop around a range in the patient, and beam-stopping points can be determined by simultaneous measurement of pair annihilation gamma rays emitted from the beams. GSI (Gesellschaft fur Schwerionenforschung) in Germany has been studying the determination of beam-stopping points in the patient using β^+ decayed nuclei (mainly ^{11}C) generated by beam nuclear fragment reaction of clinical carbon nuclei beams (stable carbon, ^{12}C) in the patient.[6,7]

In the present study, to establish optimal proton radiotherapy, the proton-irradiated area, condition, and dose distribution in the patient were examined using target nuclear fragment reaction caused by proton beams.[8–11] The positions and number of β^+ decayed nuclei were determined by simultaneous measurement using a positron emission tomography (PET) apparatus to detect pair annihilation gamma rays emitted from β^+ decayed nuclei generated by target nuclear frag-
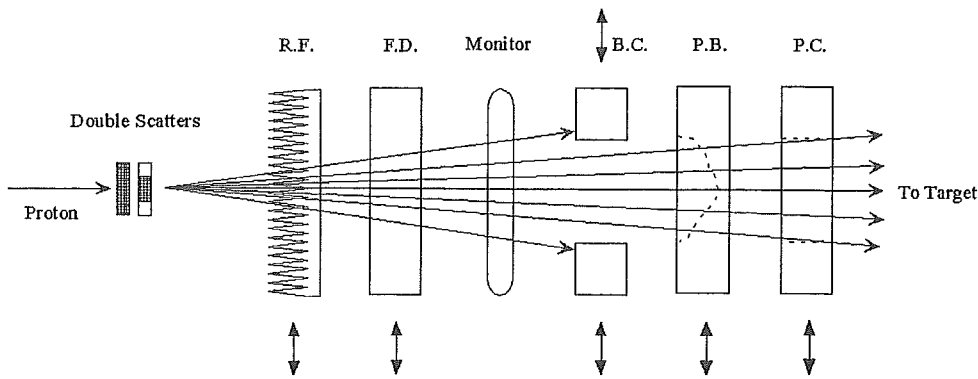
FIG. 1. Outlines of the proton irradiation apparatus.

ment reaction, and physical parameters containing information about the proton-irradiated area, condition, and the proton dose distribution were determined. The amount and distribution of β^+ decayed nuclei generated in PE (CH_2) and water (H_2O) targets by target nuclear fragment reaction after mono-energetic Bragg peak (MONO) or spread-out Bragg peak (SOBP) beam irradiation at different proton beam energies as using a PET apparatus were measured, and were compared with the calculated level. It was confirmed that the distribution of the activity could be statistically obtained by the measurement using a PET apparatus.

This paper is organized as follows. Experimental setup and procedures are described in Sec. II. Measurement and analysis results are presented in Sec. III. Section IV discusses conclusions of this study and advantage of the combination system with the use of β^+ decayed nuclei generated by the nuclear fragment reaction and PET apparatus in proton radiotherapy.

II. MATERIALS AND METHODS

A. Target nuclear fragment reaction

Target nuclear fragment reaction occurs by collision of nuclei with a relative energy of more than several tens of

megaelectron volts per nucleus, and generates β^+ decayed nuclei. The threshold energies of the reaction calculated by difference of atomic weight are 19 and 16 MeV for $^{12}C(p,pn)^{11}C$ and $^{16}O(p,pn)^{15}O$, respectively.

Since incident protons in proton beams do not fragment, target nuclear fragment reaction of nuclei in the target $X(p,x)Y$ is induced by incident protons. The reaction cross section, which depends on the relative kinetic energy of collided nuclei, increases with decreases in the energy at a relative kinetic energy of less than several hundred megaelectron volts, peaks at about 50 MeV, and then often decreases rapidly.

B. Detection of β^+ decayed nuclei generated in the target

Transport time between the proton irradiation area and PET imaging area, which were located in the same building,[12] took a minimum of 2 min.

The clinical PET apparatus (PET/Advance, GE Yokogawa Inc.) used for this study in our institution was a detection system with 12096 BGO with a crystal size of 4×8
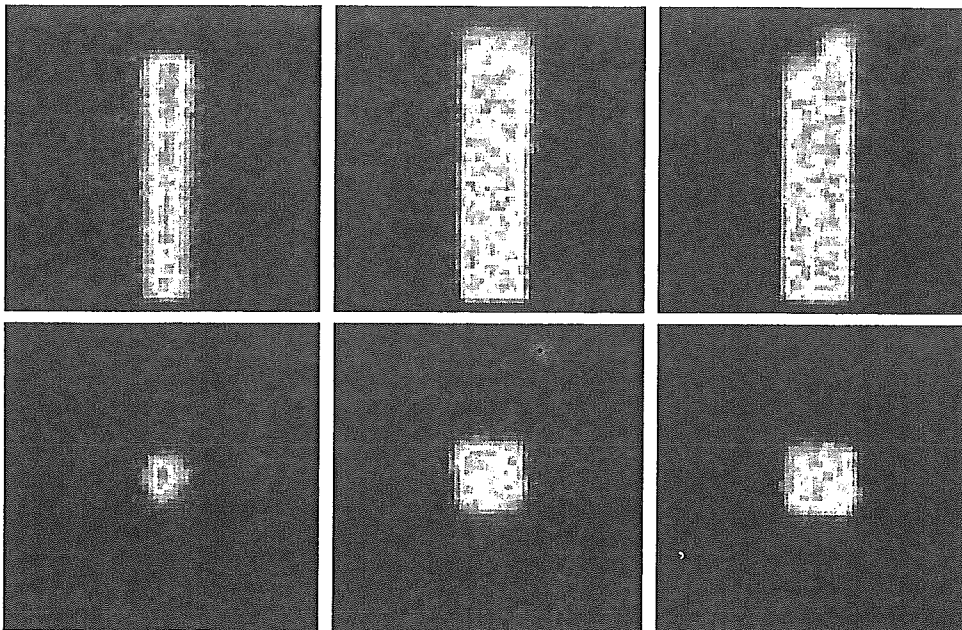

FIG. 2. Two-dimensional distributions of β^+ decayed nuclei in the PE target measured using the PET apparatus.
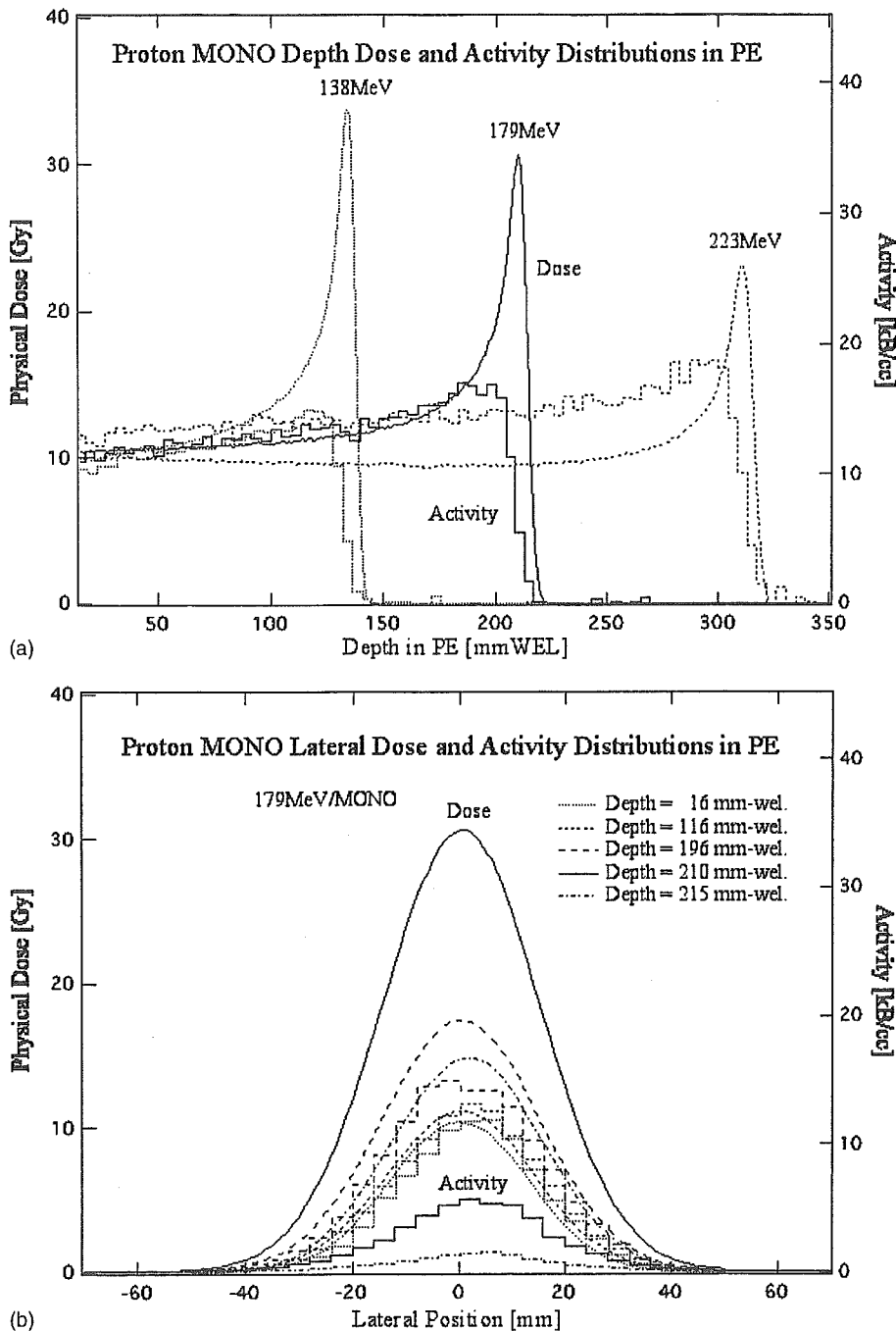
FIG. 3. Measured distributions of β^+ decayed nuclei generated in the PE target and the measured dose distributions by irradiation of MONO proton beams: (a) depth distributions at 138, 179, and 223 MeV beams, (b) lateral distributions at 179 MeV beam.

$\times 30$ mm^3 arranged on a circumference of about 900 mm in diameter. The spatial resolution after image reconstruction was 4–6 mm, which was space-dependent.

C. Experimental procedures

Proton irradiation to targets was performed using a rotation gantry port in our institution. To produce a flat irradiation field in the lateral direction, the dual ring double scattering method[13] is used for this port. To produce a flat irradiation field in the depth direction, a SOBP method with an aluminum ridge filter (RF)[14] designed according to a bi-

exponential form was used. Figure 1 shows the outlines of the apparatus for the production of the irradiation field using the port. In the figure, RF denotes the ridge filter, FD the fine degrader, BC the block collimator, PC the patient collimator, and PB the patient bolus (range compensator).

The proton beams used were MONO beams at 138, 179, and 223 MeV, and SOBP (50, 100 mm) beams at 191 MeV. The MONO beams were used with the monitor alone in the apparatus shown in Fig. 1, and the SOBP beams were used with all devices. The targets used were polyethylene (PE:CH$_2$) with density of 0.958 g/cm^3 and gelatinous water (99% pure water), and were rectangular shape of 10×10
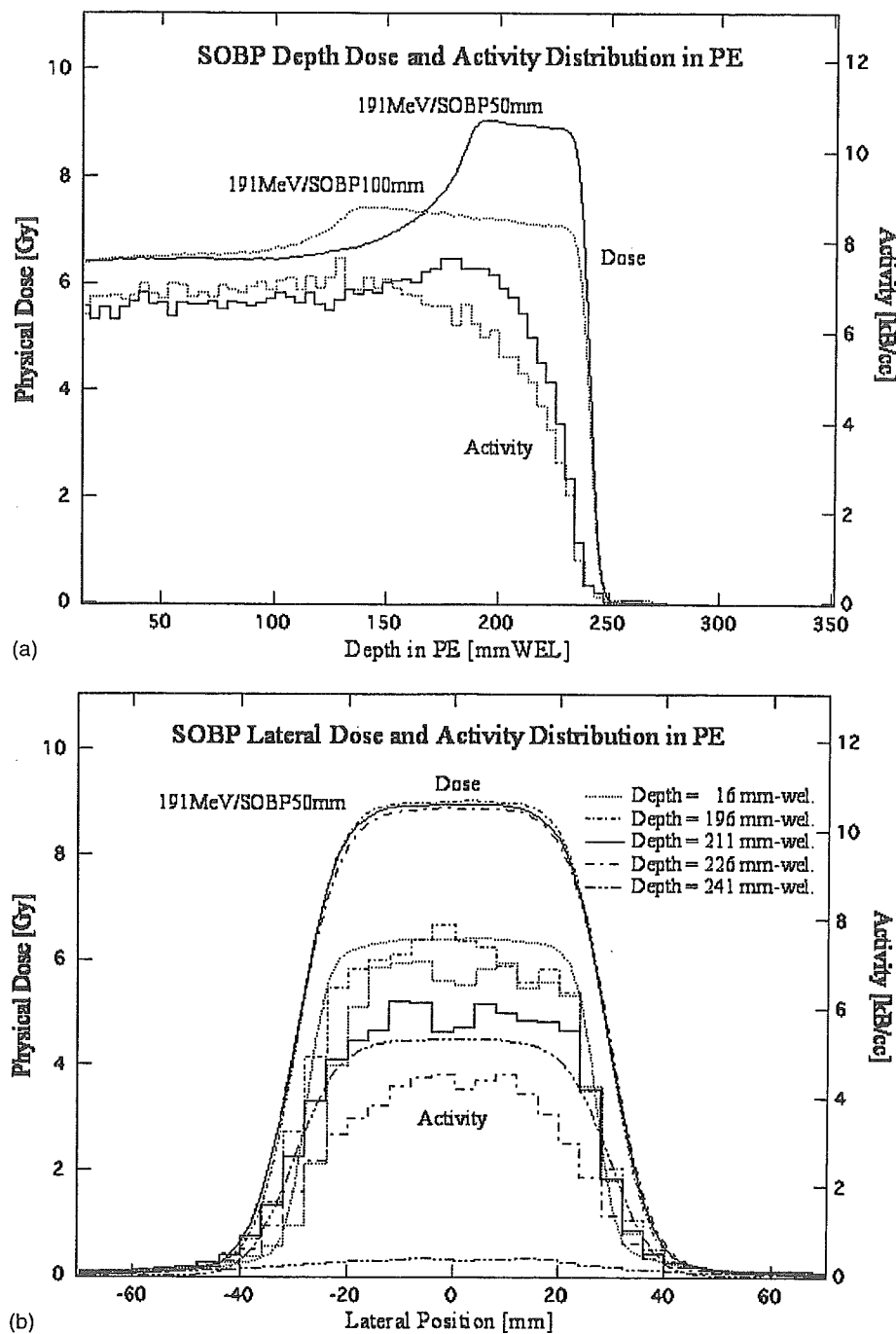
FIG. 4. Measured distributions of β^+ decayed nuclei generated in the PE target and the measured dose distributions by irradiation of SOBP proton beams at 191 MeV: (a) depth distributions in 50 and 100 mm SOBP beams, (b) lateral distributions with 50 mm SOBP beam.

×40 cm³. The MONO beam size was about 30 mm full width at half maximum (FWHM). The SOBP beams were used by collimating the irradiation field formed by dual ring double scatterers to 50 mm×50 mm. SOBP beam irradiation was also performed with a patient bolus with a 25 millimeter water equivalent length (mmWEL) range gap in half of the irradiation field (50 mm×25 mm).

MONO and SOBP beams were irradiated to the targets for 10 s and 2 min, and the irradiated doses were 10 and 7 GyE at the target entrance, respectively. PET scanning was started 2 min after irradiation and data was acquired for 2 min. The width examined by a single scanning was 144.5 mm in the depth direction, and the overlapped width was 8.5 mm. The

reconstruction of images from measurement data was performed by the two-dimensional ordered subsets-expectation maximization algorithm.[15] The spatial resolution was 4.2–5.8 mm. The changes in the activity distribution and the intensity detected between the completion of proton irradiation to the target and the start of measurement using the PET apparatus were examined.

The proton dose distributions in the depth and lateral directions were measured at intervals of 1 mm using a three-dimensional water phantom with a 75 ml farmer type chamber, and compared with the distributions of the activity measured using the PET apparatus.
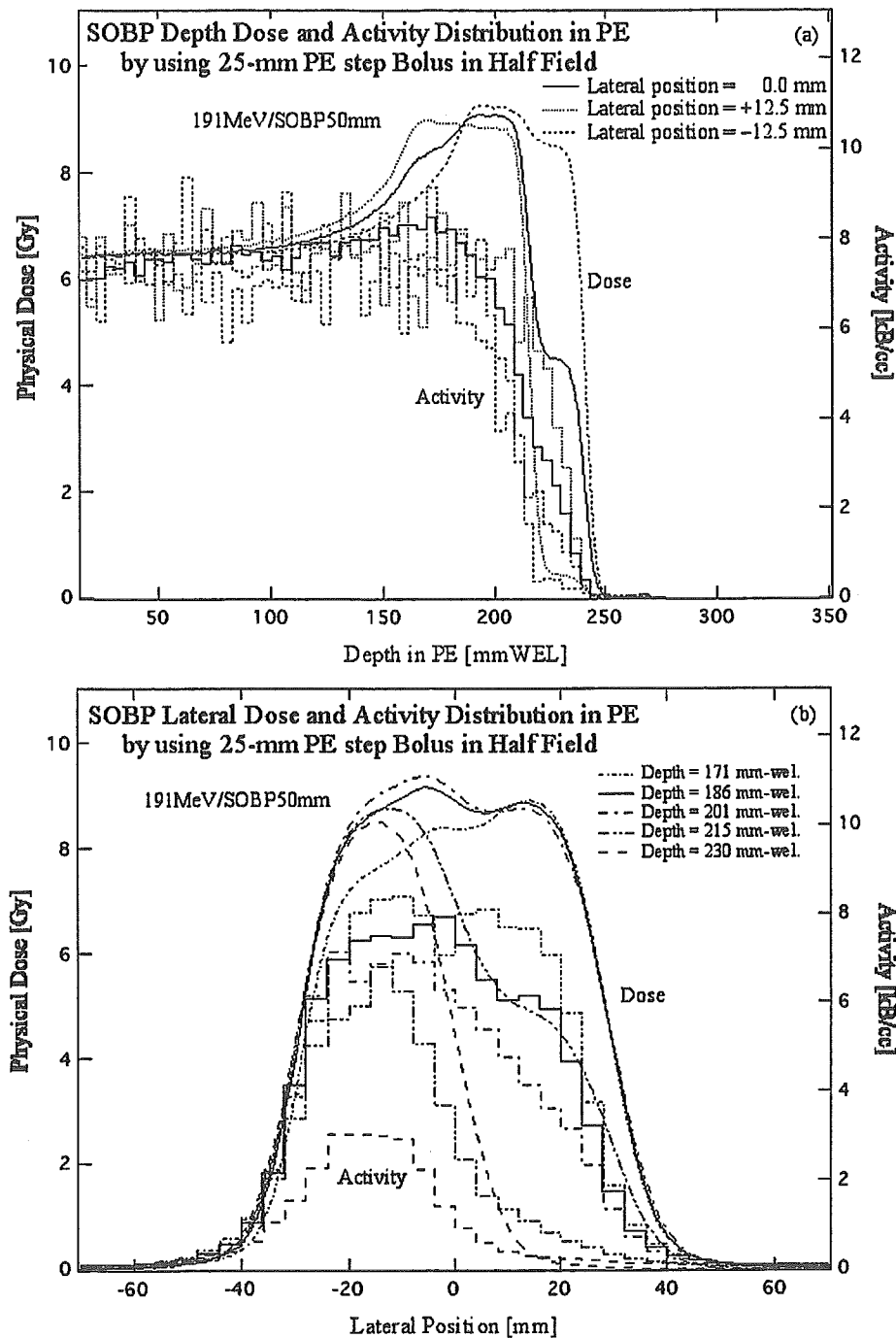
FIG. 5. Measured distributions of β^+ decayed nuclei generated in the PE target and the measured proton dose distributions by irradiation of 50 mm SOBP beams at 191 MeV with a range gap of 25 mmWEL on half of the irradiation field: (a) depth distributions, (b) lateral distributions.

III. RESULTS

A. Measured distribution of β^+ decayed nuclei generated in the PE target

Figure 2 shows the distributions of β^+ decayed nuclei generated in the PE target by irradiation of MONO beams at 179 MeV and 50 mm SOBP beams at 191 MeV, which were measured using the PET apparatus and imaged. In the figure, the left panels show the distribution of β^+ decayed nuclei by irradiation of the MONO beams, the middle panels show that by irradiation of the 50 mm SOBP beams, and the right panels show that with the range gap created with the patient bolus by irradiation of the 50 mm SOBP beams. The upper

panels show the two-dimensional distribution in the depth direction on the plane including the beam axis, and the lower panels show the two-dimensional distribution of β^+ decayed nuclei by irradiation of the MONO beams at a 150 mmWEL depth and by irradiation of the SOBP beams at a 200 mmWEL depth in the lateral direction on the plane perpendicular to the beam axis.

Based on the estimated probability of β^+ decayed nuclei generated by target nuclear fragment reaction during the period between the completion of proton irradiation and the start of measurement, the β^+ decayed nuclei were limited to ^{11}C nuclei by ^{12}C$(p,pn)^{11}$C reaction. Figure 3(a) shows the

measured distributions of β^+ decayed nuclei generated in the PE target and the measured proton dose distributions by irradiation of MONO proton beams at 138, 179, and 223 MeV. As the correction of activity with time, the half-life of ^{11}C nuclei (20.4 min) was used. Figure 3(b) shows the measured distributions of β^+ decayed nuclei generated in the PE target and the measured proton dose distributions at different depth points in the lateral direction by irradiation of MONO proton beams at 179 MeV. The stopping power and the dose-dependent activity intensity corresponding to the proton flux increased gradually with increases in the dose until the range, and then decreased rapidly. The lateral activity distribution at each depth point agreed with the proton dose distribution at the point. This was because the energy-dependent reaction cross-section term was negligible due to almost the same energy level of proton beams in the same depth region within a homogeneous target.

Figures 4(a) and 4(b) show the measured distributions of β^+ decayed nuclei generated in the PE target and the measured proton dose distributions in the depth and lateral directions, respectively, by irradiation of SOBP (50, 100 mm) beams at 191 MeV, and Figs. 5(a) and 5(b) show the measured distributions of β^+ decayed nuclei generated in the PE target and the measured proton dose distributions in the depth and lateral directions, respectively, by irradiation of SOBP (50 mm) beams at 191 MeV with a range gap of 25 mmWEL on half of the irradiation field. The distributions of β^+ decayed nuclei generated by the SOBP beam irradiation were concluded to agree with the superimposed distribution by the MONO beam irradiation, which corresponded to each value of energy loss and weight of proton flux at each point where MONO beam passes the RF with bi-exponential form, indicating a poor slope of the distributions around the range with the length of the SOBP width. The lateral distributions at the depth points showed similar shapes with the irradiation flatness. For example, 2.5 GyE SOBP (50 mm) proton beams are routinely used for clinical treatment of the head and neck region. Immediately after irradiation with the dose, activity with an intensity of about 3 kB/cc occurs in the target.

B. Measured distribution of β^+ decayed nuclei generated in the water target

As in the PE target, the measured distributions of β^+ decayed nuclei generated in the water target and the measured dose distributions by irradiation of MONO and SOBP proton beams were compared and verified. Figures 6(a) and 6(b) show the measured depth distributions of β^+ decayed nuclei generated in the water target and the measured depth dose distributions in MONO and SOBP beams. As the correction of activity with time, the half-life of ^{15}O nuclei (122.2 s) was used. It was estimated that there were many β^+ decayed nuclei generated by target nuclear fragment reaction of ^{16}O nuclei in the water target. The reaction cross section size and the long half-life of β^+ decayed nuclei determined by calculation suggested that the β^+ decayed nuclei measured using the PET apparatus in the experimental system of this study
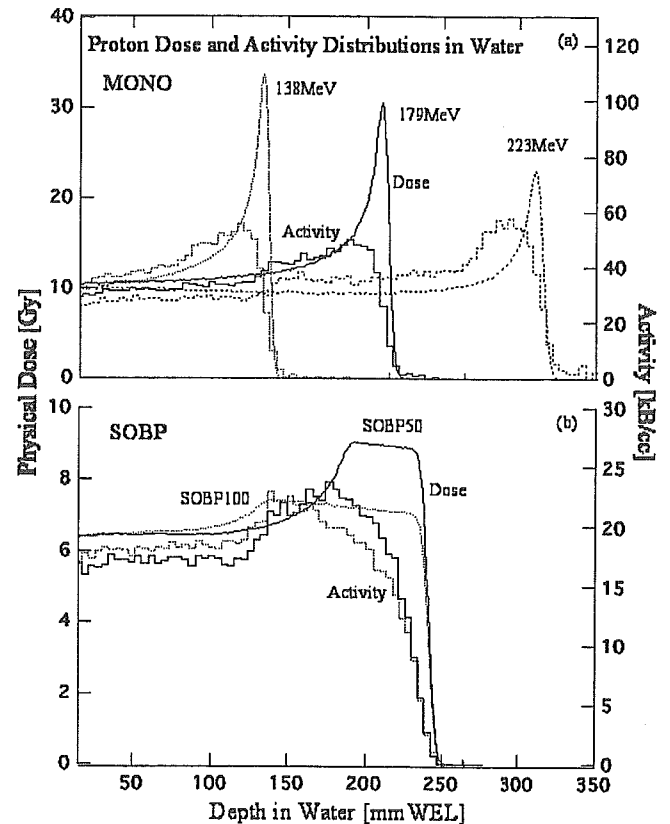
FIG. 6. Measured distributions of β^+ decayed nuclei generated in the water target and the measured dose distributions: (a) depth distributions in MONO proton beams at 138, 179, and 223 MeV, (b) depth distributions in SOBP (50, 100 mm) beams at 191 MeV.

were ^{11}C, ^{13}N (half-life, 9.97 min), and ^{15}O. Therefore, since we had to use the half-life of ^{15}O alone as the attenuation correction coefficient of activity, the measured distributions shown in the figures do not reflect the accurate amounts of β^+ decayed nuclei generated in the water target by proton irradiation. Activity with an intensity of about 15 kB/cc is induced in the target by 2.5 GyE SOBP (50 mm) proton irradiation, which is used for clinical treatment of the head and neck region. The intensity is changed from 15 to 13 kB/cc estimated with use of the half-life of ^{11}C, ^{13}N, ^{15}O, and the partial reaction cross section (see the following).

C. Calculated depth distribution of β^+ decayed nuclei generated in the PE and water targets

The distribution of β^+ decayed nuclei was calculated by the following procedures.

1. Total reaction cross section

Proton flux irradiated to the target decreases by reaction of incident protons and nuclei in the target with increases in the distance in the depth direction. The nuclear reaction rate depends on the total reaction cross section, and the reaction cross section depends on the relative kinetic energy of protons and the nuclei in the target. Figure 7 shows the experimental total reaction cross section of protons and carbon nuclei as an example. Sihver *et al.* reported the following
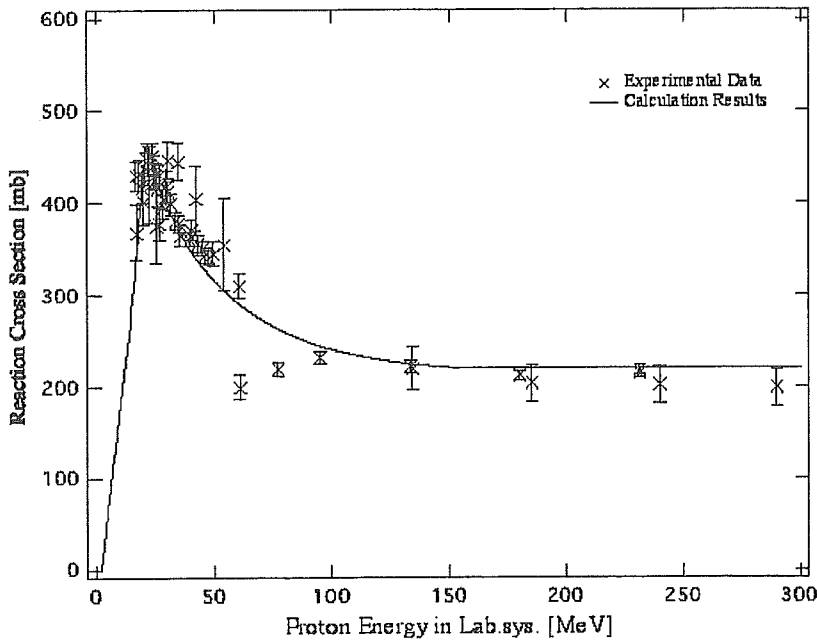
FIG. 7. Total reaction cross section of protons and carbon nuclei depending on the proton kinetic energy.

semiempirical equation, which approximately reproduces experimental measurements.[16] When the kinetic energy of proton beams E_p against target nuclei with a mass number of A_t and an atomic number of Z_t in an experimental system is $E_p \geqslant 200$ MeV, the total reaction cross section can be expressed,

$$\sigma_{\text{reac}}(E_p,A_t,Z_t) = \sigma_0(A_t) = \pi \cdot r_0^2 \cdot [1 + A_t^{1/3} - b_0 \cdot (1 + A_t^{-1/3})]^2,$$

$$b_0 = 2.247 - 0.915 \cdot (1 + A_t^{-1/3}). \tag{1}$$

Here, $r_0 = 1.36$ fm. When $E_p \geqslant 200$ MeV and $6 \leqslant Zi \leqslant 8$,

$$\sigma_{\text{reac}}(E_p,A_t,Z_t) = 0.14 \exp(0.0985 \cdot E_p)$$
$$\cdot f_{\text{reac}}(E_p,A_t,Z_t) \cdot \sigma_0(A_t). \tag{2}$$

When $20 \leqslant E_p < 150$ MeV and $6 \leqslant Z_i \leqslant 8$, and when $E_p \leqslant 150$ MeV and $Z_i < 6$ or $Z_i > 8$,

$$\sigma_{\text{reac}}(E_p,A_t,Z_t) = f_{\text{reac}}(E_p,A_t,Z_t) \cdot \sigma_0(A_t). \tag{3}$$

When $150 \leqslant E_p < 200$ MeV,

$$\sigma_{\text{reac}}(E_p,A_t,Z_t) = [f_{\text{reac}}(E_p,A_t,Z_t) \cdot g_{\text{reac}}(E_p,A_t,Z_t) + h_{\text{reac}}(E_p,A_t,Z_t)] \cdot \sigma_0(A_t). \tag{4}$$
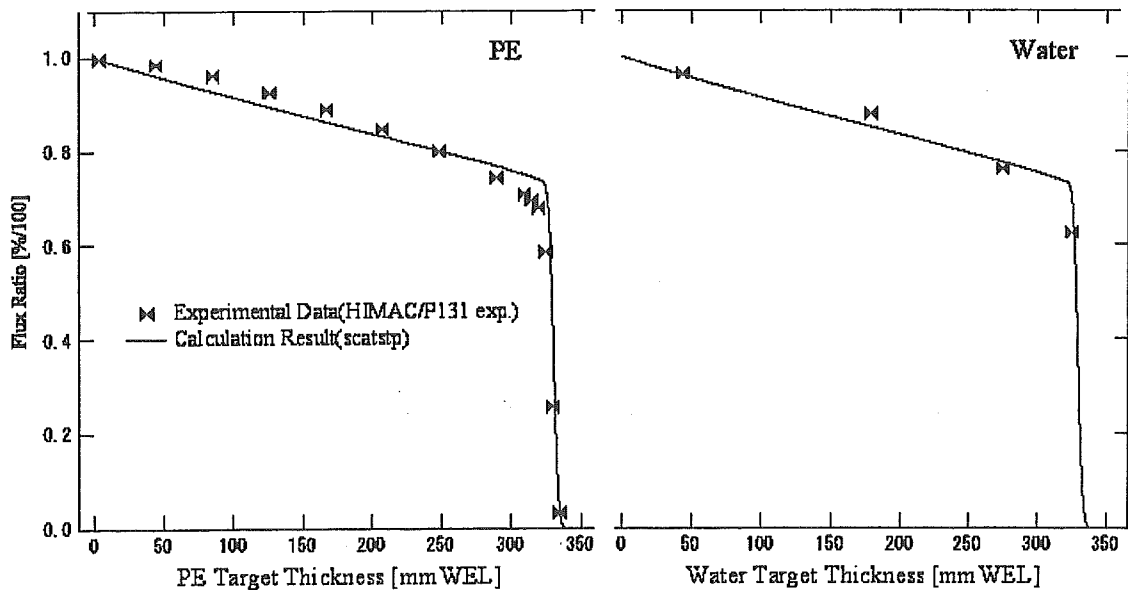

FIG. 8. Characteristics of the proton flux at different depth points in the PE and water targets. Symbols show the experimental data, and lines show the calculated results.
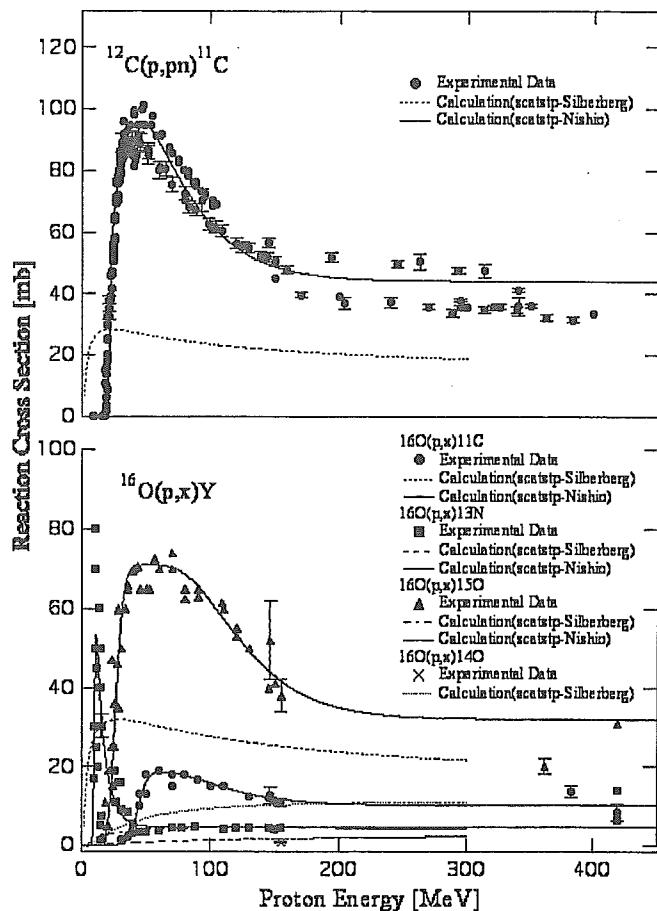
FIG. 9. Experimental and calculated partial reaction cross sections of $^{12}C(p,pn)^{11}C$ reaction, and $^{16}O(p,x)^{11}C$, ^{13}N, ^{14}O, and ^{15}O reactions.

Here, the functions f, g, and h depending on the proton beam energy and target nuclei are expressed as follows:

$$f_{reac}(E_p,A_t,Z_t) = [1.15 + \lambda_1 \exp(-E_p/\lambda_2)] \cdot [1 - 0.62$$

$$\times \exp(-E_p/200) \cdot \sin(10.9 \cdot E_p^{-0.28})],$$

$$g_{reac}(E_p,A_t,Z_t) = 4.00 - 0.02 \cdot E_p,$$

$$h_{reac}(E_p,A_t,Z_t) = 0.02 \cdot E_p - 3.00, \tag{5}$$

$$\lambda_1 = \begin{cases} 1.4(Z_t \leq 8) \\ 0(\text{otherwise}) \end{cases}, \quad \lambda_2 = \begin{cases} 38(Z_t = 4) \\ 25(Z_t = 5) \\ 10(6 \leq Z_t \leq 8) \\ 1(\text{otherwise}). \end{cases} \tag{6}$$

The total reaction cross section of protons and carbon nuclei determined using Eqs. (1)–(6) are shown in Fig. 7, indicating

TABLE I. Coefficients of Ω and η depending on the generated nuclei shown in Eq. (10).

Product	11C	13N	14O	15O
Ω	1.00	0.40	1.00	1.20
η	1.15	0.90	1.15	1.15

a relatively good reproduction of experimental measurements.

2. Calculation of proton flux

The dynamics of incident proton flux (F) in the PE and water targets were determined using the following equations with the total reaction cross section calculated using the above equations:

$$F(z,A_t,Z_t,n) = F_{in}(z = 0) \cdot q(z)$$

$$\cdot \prod \exp(-\sigma_{reac}(z,A_t,Z_t) \cdot n \cdot \Delta). \tag{7}$$

Here, E_{in} denotes the kinetic energy of incident proton beams at the target entrance, n the number of target nuclei per unit density, and Δ the target thickness. E_p is replaced by z using the following Bethe–Bloch equation of the stopping power:[17]

$$-\frac{dE_p}{dz} \approx \frac{4 \cdot \pi \cdot e^4}{m_e \cdot c^2 \cdot \beta^2} \cdot n \cdot Z_t \cdot \left\{ \ln\left(\frac{2 \cdot m_e \cdot c^2 \cdot \beta^2}{I}\right) - \ln(1 - \beta^2) - \beta^2 \right\}. \tag{8}$$

Here, I denotes the mean excitation potential, c the light velocity, β the beta value $(=v/c)$, e the electron charge, and m_e the electron mass. The range straggling effect coefficient (q) is calculated using[18]

$$q(z) = \frac{1}{\sqrt{2 \cdot \pi} \cdot \sigma_{Rst}} \cdot \int_z^\infty \exp\left(-\frac{(x-R)^2}{2 \cdot \sigma_{Rst}^2}\right) dx,$$

$$\sigma_{Rst}(R) = \sqrt{0.1569 \cdot \rho_t \cdot \frac{Z_t}{A_t} \cdot R \cdot \frac{(1 - \beta^2/2)}{1 - \beta^2}}$$

$$\cdot \left(\left(\frac{1}{\rho_t} \cdot \frac{dE}{dz}\right)_{z \to R}^{-1}\right)_{mean}. \tag{9}$$

Here, ρ_t denotes the target density. The results of the flux calculation shown in the figures have been normalized by the incident flux irradiated to the target.

Figure 8 shows the results obtained by calculation using Eqs. (1)–(9) and data of the proton flux in the PE and water targets obtained by NIRS-HIMAC/P131 experiments.[19] The calculated results almost agreed with the experimental data for both PE and water targets, although they were slightly lower in the part between the target entrance and an area near the range, and slightly higher around the range than the experimental data.

TABLE II. Coefficients of parameters depending on the generated nuclei shown in Eq. (10).

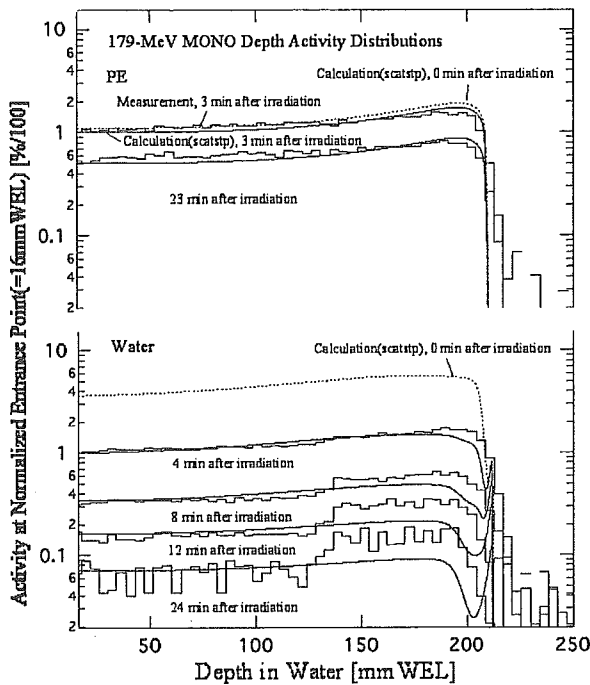| Reaction Channel		Parameter						
X	Y	a	b	c	d	e	f	g
12C	11C	96.0	21.4	0.9	0.5	1.2	39.0	2.0
16O	15O	71.0	26.0	2.8	0.6	1.1	41.0	6.0
16O	13N	66.0	10.4	0.4	0.9	0.8	11.6	1.0
16O	11C	18.8	43.6	3.6	0.5	1.0	49.0	4.0

FIG. 10. Distributions of the activity in the depth direction generated by 179 MeV MONO beam irradiation to the PE and water targets. The rectangular lines show, respectively, the distributions of the activity 3, 23 min and 4, 8, 12, 24 after proton irradiation measured using the PET apparatus. The solid lines show the corresponding distributions calculated using SCATSTP.
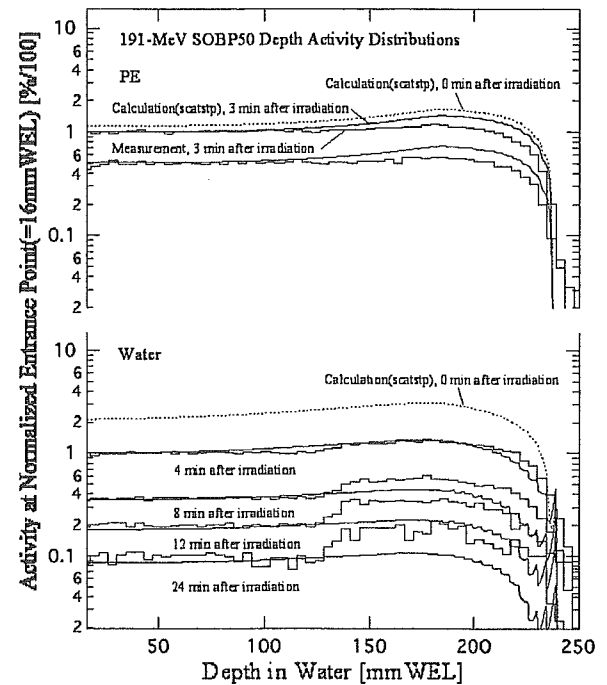
FIG. 11. Distributions of the activity in the depth direction generated by 191 MeV SOBP (50 mm) beam irradiation to the PE and water targets. The rectangular lines show, respectively, the distributions of the activity 3, 23 min and 4, 8, 12, 24 min after proton irradiation measured using the PET apparatus. The solid lines show the corresponding distributions calculated using SCATSTP.

3. Partial reaction cross section

The total cross section of reaction of incident protons and target nuclei includes partial reaction cross sections showing the degree of target nuclear fragment reaction. β⁺ decayed nuclei are contained in target nuclei fragmented by incident protons. The partial reaction cross section is an important parameter that determines the amount of β⁺ decayed nuclei generated in the target or in the patient after proton irradiation.

Figure 9 shows the experimental partial reaction cross sections of $^{12}C(p,pn)^{11}C$ reaction and $^{16}O(p,x)^{11}C$, ^{13}N, ^{14}O, and ^{15}O reactions, respectively.[20] As shown in the figures, there were variations in the experimental results, and in some reactions, the data size was small. Silberberg *et al.* reported a semiempirical equation of the partial reaction cross section.[21] $^{12}C(p,pn)^{11}C$ reaction and $^{16}O(p,x)^{11}C$, ^{13}N, ^{14}O, and ^{15}O reactions are expressed as follows:

$$\sigma_{X \to Y}(E_p)$$

$$= \sigma_R \exp\left(\begin{array}{c} -2.6 \cdot E_p^{-0.5} \cdot (A_t - A_{pr}) - 10.2 \cdot E_p^{-0.26} \\ \cdot |Z_{pr} - S \cdot A_{pr} + 5 \times 10^{-4} \cdot A_{pr}^2|^2 \end{array}\right)$$

$$\cdot \Omega \cdot \eta,$$

$$\sigma_R = \frac{232.5 \cdot (A_t^{2/3} - 1) \cdot [1 - 0.3 \cdot \ln(A_t/20)] \cdot E_p^{-0.63}}{1 - \exp(-2.6 \cdot A_t \cdot E_p^{-0.5})},$$

$$S = 0.502 - 0.26 \cdot \left(\frac{A_t}{Z_t} - 2\right)^{1.4}. \tag{10}$$

Here, A_{pr} and Z_{pr} denote the mass number and atomic number of nuclei generated by reactions, respectively. Ω and η are coefficients depending on the generated nuclei, and are shown in Table I.

TABLE III. Differences between the measured physical range and the measured or calculated activity range in the PE and water targets irradiated with proton MONO or SOBP beams at different energy levels.

	MONO						SOBP50		SOBP100	
Energy (MeV)	138	179	223	138	179	223	191		191	
R_{phy}(mm WEL)	136.0	213.5	313.5	136.0	213.5	313.5	240.8		240.8	
Target	PE	PE	PE	Water	Water	Water	PE	Water	PE	Water
R_{act}(Measurement) (mm WEL)	131.9	208.7	311.2	134.3	211.3	311.8	228.8	228.8	224.1	226.9
R_{act}(Calculation)(mmWEL)	130.6	208.5	309.4	129.1	206.6	312.2	230.3	225.3	229.1	222.6
ΔR_{act}(M.)(mmWEL)[a]	4.0	4.9	2.3	1.6	2.2	1.7	12.0	12.0	16.7	13.9
ΔR_{act}(C.)(mmWEL)[a]	5.3	5.0	4.2	6.8	7.0	1.4	10.5	15.4	11.7	18.2

[a]$\Delta R_{act} = R_{phy} - R_{act}$

TABLE IV. FWHM of the dose and activity distributions in the PE and water targets irradiated with 179 MeV proton MONO beams and the difference.

Energy (MeV)		MONO 179				
Target		PE			Water	
	FWHM [mm]		ΔFWHM [mm][a]	FWHM(mm)		ΔFWHM (mm)[a]
Depth (mm WEL)	Dose	Activity		Dose	Activity	
16	30.9	31.0	0.1	30.9	31.6	0.7
116	32.4	33.0	0.6	32.4	31.8	-0.6
196	34.7	34.8	0.1	34.7	34.3	-0.4
210	34.9	32.6	-2.3	34.9	34.4	-0.5
215	33.6	35.2	1.6	33.6	34.0	0.4

[a]FWHM(Activity)-FWHM(Dose).

Figure 9 shows the partial reaction cross sections of $^{12}C(p,pn)^{11}C$ reaction and $^{16}O(p,x)^{11}C$, ^{13}N, ^{14}O, and ^{15}O reactions calculated using Eq. (10), respectively. There were large differences in the partial reaction cross sections at an energy level of less than 250 MeV, which is required for proton radiotherapy, between the experimental and calculated results. Therefore, we developed a simple equation of more accurate reproduction of experimental partial reaction cross sections, as follows:

$$\sigma_{X \to Y}(E_p) = \frac{a}{1 + \exp\left(\dfrac{b - E_p}{c}\right)} \cdot \left\{1 - d \cdot \left(1 - e\right.\right.$$
$$\times \left.\left.\exp\left(-\frac{E_p - f}{g}\right)\right)^h\right\}. \tag{11}$$

Here, the coefficients of parameters depending on the generated nuclei used in Eq. (11) are shown in Table II.

The calculation of partial reaction cross sections using Eqs. (10) and (11) was performed with the program SCATSTP.

4. Distribution of the generated nuclei

Since there is no time structure with proton beams in a cyclotron within the target irradiation time, the intensity of proton beams is regarded as constant, and the generation rate of positron-emitting nuclei is constant. When the half-life of β^+ decayed nuclei is denoted by $T_{1/2}$, and the beam irradia-

tion time by t_i, the total number of β^+ decayed nuclei generated during the beam irradiation period N_R is expressed as follows:

$$N_R(t_i, F, \sigma_{X \to Y}) = F(z, A_t, Z_t, n)$$
$$\cdot [1 - \exp(-\sigma_{X \to Y}(E_p) \cdot n \cdot \Delta)]. \tag{12}$$

The number of residual positron-emitting nuclei in the target immediately after irradiation N_{act} determined by taking into consideration the decrease in the number of positron-emitting nuclei depending on the half-life is expressed as follows:

$$N_{act}(t_i, T_{1/2}, F, \sigma_{X \to Y}) = N_R(t_i, F, \sigma_{X \to Y}) \cdot \left[1 + 2^{-t_i/T_{1/2}}\right.$$
$$\left. - \frac{T_{1/2}}{t_i \cdot \ln 2} \cdot (1 - 2^{-t_i/T_{1/2}})\right]. \tag{13}$$

When the time between the completion of irradiation and the start of measurement using a PET apparatus is denoted by t_s, the time between the completion of irradiation and that of measurement by t_e, the detection efficiency at single 511 keV gamma ray by ε, and the solid angle of the total detectors by Ω_{sa}, the number of activities detected by the PET apparatus is expressed as follows:

TABLE V. Changes in the measured physical range, the measured and calculated activity range, and their differences in the PE and water targets after irradiation of 179 MeV proton MONO beams or 191 MeV proton SOBP (50 mm) beams.

Energy (MeV)	MONO 179						SOBP50 191					
R_{phy} (mmWEL)	213.5						240.8					
Target	PE	PE	Water	Water	Water	Water	PE	PE	Water	Water	Water	Water
Time after irradiation (min)	3	23	4	8	12	24	3	23	4	8	12	24
R_{act} (Measurement) (mmWEL)	208.7	208.7	211.3	209.6	205.3	200.9	228.8	229.4	228.8	229.4	228.8	229.4
R_{act} (Calculation) (mmWEL)	208.5	208.5	206.6	206.0	195.3	195.0	230.3	230.3	225.3	221.4	221.2	219.0
ΔR_{act} (M.) [mmWEL][a]	4.9	4.8	2.2	3.9	8.2	12.6	12.0	11.4	12.0	11.4	12.0	11.4
ΔR_{act} (C.) [mmWEL][a]	5.0	5.0	7.0	7.5	18.2	18.5	10.5	10.5	15.4	19.4	19.6	21.8

[a]$\Delta R_{act} = R_{phy} - R_{act}$.

$$N_{\mathrm{PET}}(t_i, T_{1/2}, t_s, t_e, F, \sigma_{X \to Y})$$

$$= N_{\mathrm{act}}(t_i, T_{1/2}, F, \sigma_{X \to Y}) \cdot 2^{-t_s/T_{1/2}}$$

$$\cdot [1 - 2^{-(t_e - t_s)/T_{1/2}}] \cdot \varepsilon^2 \cdot \frac{\Omega_{\mathrm{sa}}}{4 \cdot \pi}. \tag{14}$$

The distribution of the activity in the depth direction generated by 179 MeV MONO beam irradiation to the PE and water targets was measured using the PET apparatus, and determined using Eq. (14) based on the partial reaction cross sections calculated using Eq. (11), of which the results are shown in Fig. 10. In the figures, the temporal changes in the measured and calculated distributions of the activity after irradiation are shown. The measured and calculated distributions of the activity were normalized by the distribution at 16 mmWEL distant from the beam entrance of the target in the depth direction 3 min after irradiation. In the distributions of the activity, not the activity remaining in the target but the decreased activity detected by the PET apparatus is reflected. In the PE target, the distributions immediately (calculation alone), 3, and 23 min after irradiation are shown, and in the water target, the distributions immediately (calculation alone), 4, 8, 12, and 24 min after irradiation are shown. Since the activity in the PE target was almost due to ^{11}C alone from 3 min after irradiation, the activity 23 min after irradiation was half of that 3 min after irradiation with a similar distribution shape. In the water target, the activity was due to ^{11}C, ^{13}N, ^{14}O, and ^{15}O, and the distribution shape was changed. The distributions of the activity measured using the PET apparatus slightly differ from the calculated distributions, which may be caused mainly by the measurement and calculation accuracy of the partial reaction cross section, which is the core for the calculation of distributions and the calculation accuracy of flux in the target. The distal regions in the measured distributions may affect the differences in the distributions depending on the accuracy of the PET apparatus and the algorithm of image reconstruction.

Figure 11 shows the measured and calculated distributions of the activity in the depth direction generated by 191 MeV SOBP (50 mm) irradiation to the PE and water targets, respectively. Since the proton dose distribution of SOBP beams is produced by superimposing MONO beams, the distribution of the activity by SOBP beam irradiation can also be shown by superimposing the distribution of the activity by MONO beam irradiation. Therefore, the difference in the distribution of the activity between measurement and calculation was larger by SOBP beam irradiation than by MONO beam irradiation.

Table III summarizes the measured physical range (R_{phy}), the measured and calculated activity range (R_{act}), which was defined as the 50% peak-normalized depth point, and their differences (ΔR_{act}), in the PE and water targets irradiated with 138, 179, or 223 MeV proton MONO beams or 191 MeV proton SOBP (50, 100 mm) beams. The maximal ΔR_{act} was about 5 mmWEL, and the ΔR_{act} was slightly larger in the water target than in the PE target. Moreover, there was a tendency for the range difference to become small for the range straggling effect in proportion to the in-

cident proton energy. The measurements of the activity range using the PET apparatus included a random error of about ±1 mm in the target position, against the apparatus position, with each proton energy level and each MONO or SOBP irradiation.

Table IV summarizes the FWHM of the dose and activity distributions in the PE and water targets irradiated with 179 MeV proton MONO beams and their differences. Some measurement points showed a difference of about 2 mm in the PE target, which may have been caused by the spatial resolution of the PET apparatus, but it was confirmed that the other measurement points were reproduced at an accuracy within a difference of less than 1 mm.

Table V summarizes the changes in the measured physical range, the measured and calculated activity range, and their differences in the PE and water targets after irradiation of 179 MeV proton MONO beams or 191 MeV proton SOBP (50 mm) beams. In the PE target, there were almost no changes in the difference between the physical and activity ranges after proton irradiation, which were within the measurement error. In the water target, the difference between the physical and activity ranges tended to increase gradually after proton irradiation, and this tendency was marked with proton MONO irradiation. The changes were 2–13 mmWEL by measurement and 7–19 mmWEL by calculation. Although there was a difference in the numerical value between the measurement and calculation, the changes determined by the two methods were similar (about 11 mmWEL). After proton SOBP irradiation, almost no changes in the measured range difference were observed, but the calculated difference was 7 mmWEL. Since the intensity of the MONO beams irradiated to the target was low, the activity depended on the half-lives of generated nuclei, and the percentage of ^{15}O (and ^{14}O) at the start of measurement using the PET apparatus was markedly higher by proton MONO irradiation than by proton SOBP irradiation. Therefore, the difference in the changes in the range difference after proton SOBP irradiation between the measurement and calculation may have been caused by the calculation accuracy of the partial reaction cross sections and proton flux affected by the different percentages of generated nuclei. The decrease in the statistical accuracy of the gradually decreased activity and the resultant worsening of the spatial resolution may also have affected the measurement using the PET apparatus.

IV. DISCUSSION AND CONCLUSIONS

The distribution of β^+ decayed nuclei generated in the therapeutic proton-irradiated targets by nuclear fragment reaction was measured using a PET apparatus, which was located in another room apart from the room with the proton irradiation apparatus, and the activity distribution was obtained. It was confirmed that the activity obtained was 3 kB/cc in the PE target and 13 kB/cc in the water target, taking the condition and dose of proton beams used for clinical treatment into consideration. It was also confirmed that there were differences in the distributions of the activity by irradiation of MONO and SOBP (50, 100 mm) beams at different energy levels to the PE and water targets between the
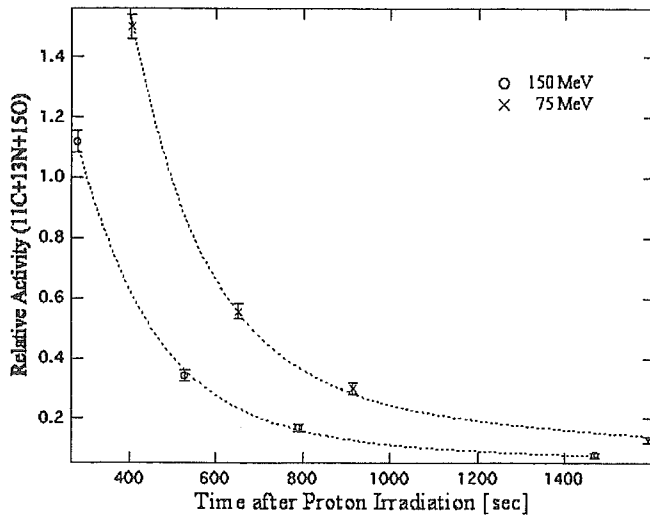
FIG. 12. Intensity decay data of the activity for the $^{16}O(p,x)^{11}C$, ^{13}N, and ^{15}O reactions at 75, and 150 MeV proton energies. Dash lines are fitting results by Eq. (A1).

measurement using the PET apparatus and the calculation. With regard to the relationship between the measured proton dose distribution and the activity distribution, the activity range was several mmWEL shorter than the physical range, and depended on the targets. In the water target, the difference tended to be large with the time between the completion of proton irradiation and the start of measurement using the PET apparatus. The FWHM in the measured lateral distributions of the irradiation dose and activity agreed at an accuracy within 1 mm.

The precision of the calculation of the activity distribution is insufficient in the agreement with the measured distribution using PET apparatus at present. In the future, it is necessary to improve the precision of the calculation, and the spatial resolution by the PET apparatus itself and the image reconstruction algorithm. Information about the kinds and percentages of target nuclei is required for the calculation of the activity distribution, and information about the CT values determined mainly by the electron density, which are currently used for the calculation of irradiation doses, is insufficient for clinical treatment, but currently, there is no other way but the use of the information about general anatomic structures linked to the CT values of clinical images. The development of techniques using double energy x rays by a synchrotron light source,[22] on which studies have been ad-

vancing, is expected, because with such techniques, the kinds of nuclei constituting the patient could be determined.

Since there was a problem in the accuracy of the calculation of the absolute activity distribution using the proton dose distribution, it was difficult to evaluate the results, but the activity distribution is very useful. For examples, beam on-line PET system is able to monitor the changes in the tumor and the proton-irradiated area after every proton irradiation. Research and development of the beam on-line PET system are our next study, and it has already started.

ACKNOWLEDGMENTS

APPENDIX: RATE OF PARTIAL REACTION CROSS SECTION FOR $^{16}O(P,X)^{11}C$, ^{13}N, AND ^{15}O REACTIONS

Percentage of the generated ^{14}O nucleus occupied in total generated nuclei by the target fragment reaction $^{16}O(p,x)$ is estimated to be small in less than 3% by use of ratio of the partial reaction cross section in Eq. (11) and the half-life (70.6 s) of the ^{14}O nucleus. Therefore, the ratio of the partial reaction cross section of the $^{16}O(p,x)^{11}C$, ^{13}N, and ^{15}O reactions is calculated by fitting intensity decay data of measured activity shown in Fig. 10, and is expressed as follows:

$$\sigma_{16O \to 11C,13N,15O}(E_p)$$

$$\to 6.56 \cdot \sigma_{16O \to 11C}(E_p) \cdot \left(\frac{1}{2}\right)^{t/[T_{1/2}(11C)]}$$

$$+ 12.91 \cdot \sigma_{16O \to 13N}(E_p) \cdot \left(\frac{1}{2}\right)^{t/[T_{1/2}(13N)]}$$

$$+ 48.01 \cdot \sigma_{16O \to 15O}(E_p) \cdot \left(\frac{1}{2}\right)^{t/[T_{1/2}(15O)]}$$

$$\propto N_{PET}(t,E_p). \tag{A1}$$

TABLE VI. Ratio of the partial reaction cross section for the $^{16}O(p,x)^{11}C$, ^{13}N, and ^{15}O reactions at 75 and 150 MeV proton energies.

	$\sigma_{16O \to 11C}(E_p) / \sigma_{16O \to 15O}(E_p)$		$\sigma_{16O \to 13N}(E_p) / \sigma_{16O \to 15O}(E_p)$	
Energy: E_p (MeV)	75	150	75	150
Measurement	0.19	0.26	0.03	0.01
Calculation (SCATSTP)	0.26	0.28	0.07	0.11
Meas/Calc	0.75	0.94	0.40	0.08

o

Each coefficient of the equation is determined by use of the half-life of ^{11}C, ^{13}N, and ^{15}O nuclei, the number of residual positron-emitting nuclei in the target immediately after irradiation N_{act} is shown in Eq. (13) , and the intensity decay of activity in measurement time for 2 min by the PET apparatus. The number of activities detected by the PET apparatus N_{PET} is shown in Eq. (14) .

Figure 12 shows the intensity decay data of the measured activity for the ^{16}O$(p,x)^{11}$C, ^{13}N, and ^{15}O reactions at 75 and 150 MeV proton energies, and the fitting result by Eq. (A1). The ratio of the partial reaction cross section $\sigma_{16O \rightarrow 11C}/\sigma_{16O \rightarrow 15C}$, $\sigma_{16O \rightarrow 13N}/\sigma_{16O \rightarrow 15C}$ by the fitting result and the calculation result in Eq. (11) is summarized in Table VI. Differences of both results were large, especially in the ratio of partial reaction cross section $\sigma_{16O \rightarrow 13N}/\sigma_{16O \rightarrow 15C}$ for the generated ^{13}N nucleus.

[a]Electronic mail: tnishio@east.ncc.go.jp

[1]PARTICLES 34 PTCOG Newsletter, July, 2004.

[2]I. Tanihata, H. Hamagaki, O. Hashimoto, Y. Shida, and N. Yoshikawa, "Measurements of interaction cross sections and nuclear radii in the light p-shell region," Phys. Rev. Lett. **55**, 2676–2679 (1985).

[3]C. A. Tobias, E. V. Benton, M. P. Capp, A. Chatterjee, M. R. Cruty, and R. P. Henke, "Particle radiography and autoactivation," Int. J. Radiat. Oncol., Biol., Phys. **3**, 35–44 (1977).

[4]M. Kanazawa, A. Kitagawa, S. Kouda, T. Nishio, M. Torikoshi, K. Noda, T. Murakami, M. Suda, T. Tomitani, K. Kanai, Y. Futami, M. Shinbo, E. Urakabe, and Y. Iseki, "Application of an RI-beam for cancer therapy: In-vivo verification of the ion-beam range by means of positron imaging," Nucl. Phys. A **701**, 244c–252c (2002).

[5]H. Mizuno, T. Tomitani, M. Kanazawa, A. Kitagawa, J. Pawelke, Y. Iseki, E. Urakabe, M. Suda, A. Kawano, R. Iritani, S. Matsushita, I. Inaniwa, T. Nishio, S. Furukawa, K. Ando, Y. K. Nakamura, T. Kanai, and K. Ishii, "Washout measurement of radioisotope implanted by radioactive beam in the rabbit," Phys. Med. Biol. **48**, 2269–2281 (2003).

[6]J. Pawelke, L. Byars, W. Enghardt, W. D. Fromm, H. Geissel, B. G. Hasch, K. Lauckner, P. Manfraß, D. Schardt, and M. Sobiella, "The investigation of different cameras for in-beam PET imaging," Phys. Med. Biol. **41**, 279–296 (1996).

[7]D. Schardt, I. Schall, H. Geissel, H. Irnich, G. Kraft, A. Magel, M. F. Mohar, G. Munzenberg, F. Nickel, C. Scheidenberger, W. Schwab, and L. Sihver, "Nuclear fragmentation of high-energy heavy-ion beams in water," Adv. Space Res. **17**, 87–94 (1996).

[8]T. Nishio, M. Shimbo, T. Murakami, and T. Ogino, "A study of β^+ de-

cayed nucleus produced from target fragmentation by using a proton beam for therapy," Jpn. J. Med. Phys. Proc. JSMP2001 **21**, 119–120 (2001).

[9]K. Parodi, W. Enghardt, and T. Haberer, "In-beam PET measurements of β^+ radioactivity induced by proton beams," Phys. Med. Biol. **47**, 21–36 (2002).

[10]D. W. Litzenberg, D. A. Roberts, M. Y. Lee, K. Pham, A. M. Vander Molen, R. Ronningen, and F. D. Becchetti, "On-line monitoring of radiotherapy beams: Experimental results with proton beams," Med. Phys. **26**, 992–1006 (1999).

[11]T. Nishio, T. Ogino, M. Shimbo, S. Katsuta, S. Kawasaki, T. Murakami, T. Sato, Y. Kojima, K. Murakami, and H. Ikeda, "Distributions of β^+ decayed nucleus produced from the target fragment reaction in (CH$_2$)n and patient liver targets by using a proton beam for therapy," Abstracts of the XXXIV PTCOG Meeting, Boston, 15–16, June 2001.

[12]T. Nishio, "Proton therapy facility at National Cancer Center, Kashiwa, Japan," J. At. Energy Soc. **41**, 1134–1138 (1999).

[13]A. M. Koehler, R. J. Schneider, and J. M. Sisterson, "Flattening of proton dose distributions for large-field radiotherapy," Med. Phys. **4**, 297–301 (1977).

[14]W. T. Chu, B. A. Ludewigt, and T. R. Renner, "Instrumentation for Treatment of Cancer Using Proton and Light-Ion Beams," LBL-33403/UC-406, 1993.

[15]H. M. Hudson and R. Larkin, "Accelerated image reconstruction using ordered subsets of projection data," IEEE Trans. Med. Imaging **MI-13**, 601–609 (1994).

[16]L. Sihver, C. H. Tsao, R. Silberberg, T. Kanai, and A. F. Barghouty, "Total reaction and partial cross section calculations in proton-nucleus and nucleus-nucleus reactions," Phys. Rev. C **47**, 1225–1236 (1993).

[17]ICRU Report 49, "Stopping powers and ranges for protons and alpha particles," 1993.

[18]M. G. Payne, "Energy straggling of heavy charged particles in thick absorbers," Phys. Rev. **185**, 611–623 (1969).

[19]T. Nishio, T. Inaniwa, M. Kanazawa, A. Kitagawa, T. Murakami, T. Kanai, T. Tomitani, M. Suda, E. Urakabe, M. Hirai, H. Mizuno, and T. Kohno, "A study of the autoactivation in target by using a proton beam and the beam ON LINE type positron CAMERA," Anunual Report of the Research Project with Heavy Ions at NIRS-HIMAC, 2002, pp. 272–274; 2003, pp. 234–236.

[20]A. S. Iljinov, V. G. Semenov, M. P. Semenova, and H. Schopper, "Interactions of protons with nuclei (supplement to I/13a,b,c)," Landolt-Bornstein New Series, 1994.

[21]R. Silberberg and C. H. Tsao, "Partial cross-sections in high-energy nuclear reactions, and astrophysical applications," Astrophys. J., Suppl. **25**, 315–333 (1973).

[22]M. Torikoshi, T. Tsunoo, T. Tsunoo, M. Endo, K. Uesugi, and N. Yagi, "Design of synchrotron light source and its beamline dedicated to dual-energy x-ray computed tomography," J. Biomed. Opt. **6**, 371–377 (2001).

O R I G I N A L R E P O R T

Phase II Study of Radiotherapy Employing Proton Beam for Hepatocellular Carcinoma

Mitsuhiko Kawashima, Junji Furuse, Teiji Nishio, Masaru Konishi, Hiroshi Ishii, Taira Kinoshita, Michitaka Nagase, Keiji Nihei, and Takashi Ogino

A B S T R A C T

Purpose
To evaluate the safety and efficacy of proton beam radiotherapy (PRT) for hepatocellular carcinoma.

Patients and Methods
Eligibility criteria for this study were: solitary hepatocellular carcinoma (HCC); no indication for surgery or local ablation therapy; no ascites; age ≥ 20 years; Zubrod performance status of 0 to 2; no serious comorbidities other than liver cirrhosis; written informed consent. PRT was administered in doses of 76 cobalt gray equivalent in 20 fractions for 5 weeks. No patients received transarterial chemoembolization or local ablation in combination with PRT.

Results
Thirty patients were enrolled between May 1999 and February 2003. There were 20 male and 10 female patients, with a median age of 70 years. Maximum tumor diameter ranged from 25 to 82 mm (median, 45 mm). All patients had liver cirrhosis, the degree of which was Child-Pugh class A in 20, and class B in 10 patients. Acute reactions of PRT were well tolerated, and PRT was completed as planned in all patients. Four patients died of hepatic insufficiency without tumor recurrence at 6 to 9 months. Three of these four patients had pretreatment indocyanine green retention rate at 15 minutes of more than 50%. After a median follow-up period of 31 months (16 to 54 months), only one patient experienced recurrence of the primary tumor, and 2-year actuarial local progression-free rate was 96% (95% CI, 88% to 100%). Actuarial overall survival rate at 2 years was 66% (48% to 84%).

Conclusion
PRT showed excellent control of the primary tumor, with minimal acute toxicity. Further study is warranted to scrutinize adequate patient selection in order to maximize survival benefit of this promising modality.

J Clin Oncol 23:1839-1846. © 2005 by American Society of Clinical Oncology

INTRODUCTION

Cirrhosis is found in more than 80% of patients with hepatocellular carcinoma (HCC). This precludes more than 70% of the patients from receiving potentially curative treatments, and also contributes eventually to fatal hepatic insufficiency and multifocal tumorigenesis.[1,2] Approximately 50% to 70% and 30% to 50% of 5-year overall survival was achieved with surgery including liver transplantation[3-6] and percutaneous local ablation,[7-9] respectively, for an adequately selected population of patients. However, no standard strategy has been established for patients with unresectable HCC at present.

Partial liver irradiation for HCC using 50 to 70 Gy of megavoltage x-ray with or without transarterial chemoembolizaztion (TACE) for 5 to 7 weeks has been widely applied during the last two decades. This resulted in response rates of 33% to 67%, with a median survival period of 13 to 19

months and 10% to 25% overall survival at 3 years.[10-12] Since 1985, proton radiotherapy (PRT) administered at a median dose of 72 cobalt gray equivalent (Gy$_E$) in 16 fractions during 3 weeks with or without TACE, had been applied in more than 160 patients with HCC at the University of Tsukuba, resulting in a more than 80% local progression-free survival rate with 45% and 25% overall survival at 3 and 5 years, respectively.[13,14] The excellent depth-dose profile of the proton beam enabled us to embark on an aggressive dose escalation while keeping a certain volume of the noncancerous portion of the liver free from receiving any dose of irradiation. This single-institutional, single-arm, prospective study was conducted to confirm encouraging retrospective results of PRT for HCC using our newly installed proton therapy equipment.

PATIENTS AND METHODS

Patient Population

Patients were required to have uni- or bidimensionally measurable solitary HCC of $\leq$ 10 cm in maximum diameter on computed tomography (CT) and/or magnetic resonance (MRI) imaging. In addition, the following eligibility criteria were required: no history of radiotherapy for the abdominal area; no previous treatment for HCC within 4 weeks of inclusion; no evidence of extrahepatic spread of HCC; age $\geq$ 20 years; Zubrod performance status (PS) of 0 to 2; WBC count $\geq$ 2,000/mm^3; hemoglobin level $\geq$ 7.5 g/dL; platelet count $\geq$ 25,000/mm^3; and adequate hepatic function (total bilirubin $\leq$ 3.0 mg/dL; AST and ALT < 5.0× upper limit of normal; no ascites). Patients who had multicentric HCCs were not considered as candidates for this study, except for those with the following two conditions: (1) multinodular aggregating HCC that could be encompassed by single clinical target volume; (2) lesions other than targeted tumor that were judged as controlled with prior surgery and/or local ablation therapy. Because a planned total dose would result in a significant likelihood of serious bowel complications, patients who had tumors abutting or invading the stomach or intestinal loop were excluded. The protocol was approved by our institutional ethics committee, and written informed consent was obtained from all patients.

Pretreatment Evaluation

All patients underwent indocyanine green clearance test, and the retention rate at 15 minutes (ICG R15) was measured for the purpose of quantitative assessment of hepatic functional reserve. CBC, biochemical profile including total protein, albumin, total cholesterol, electrolytes, kidney and liver function tests, and serological testing for hepatitis B surface antigen and antihepatitis C antibody were done. C-reactive protein and tumor markers including alpha feto-protein and carcinoembryonic antigen were also measured. Chest x-ray was required to exclude lung metastasis. All patients were judged as unresectable by expert hepatobiliary surgeons in our institution, based on their serum bilirubin level, ICG R15, and expected volume of resected liver.[15] Gastrointestinal endoscopy was done to exclude active ulcer and/or inflammatory disease located at the stomach and the duodenum. All patients underwent abdominal ultrasonography, triphasic CT or

MRI, CT during arteriography and arterial portography.[16] Diagnosis of HCC was based on radiographic findings on triphasic CT/MRI. Radiologic criteria for HCC definition were as follows: tumor showing high attenuation during hepatic arterial and portal venous phase indicating hypervascular tumor; tumor showing low attenuation during delayed phase indicating rapid wash-out of contrast media. Confirmatory percutaneous fine-needle biopsies were required for all patients unless they had radiologically compatible, postsurgical recurrent HCC. Tumors that broadly abut on the vena cava, portal vein, or hepatic vein that were associated with caliber changes and/or filling defects of these vessels, were tentatively defined as positive for macroscopic vascular invasion. One patient had visible tumor on fluoroscopy because of residual iodized oil contrast medium used in previous TACE. For the other 29 patients, one or two metallic markers (inactive Au grain of which the diameter and length were 1.1 mm and 3.0 mm, respectively) were inserted percutaneously at the periphery of the target tumor.

Treatment Planning

PRT was performed with the Proton Therapy System (Sumitomo Heavy Industries Ltd, Tokyo, Japan), and treatment planning, with the PT-PLAN/NDOSE System (Sumitomo Heavy Industries Ltd). In this system, the proton beam was generated with Cyclotron C235 with an energy of 235 MV at the exit. Gross tumor volume (GTV) was defined using a treatment planning CT scan using X Vision Real CT scanner (Toshiba Co Ltd, Tokyo, Japan), and clinical target volume (CTV) and planning target volume (PTV) were defined as follows: CTV = GTV + 5 mm, and PTV = CTV + 3 mm of lateral, craniocaudal, and anteroposterior margins. Proton beam was delivered with two-beam arrangement to minimize irradiated volume of noncancerous liver using our rotating gantry system. The beam energy and spread-out Bragg peak[13] were fine-tuned so that 90% isodose volume of prescribed dose encompassed PTV. To evaluate the risk of radiation-inducing hepatic insufficiency, dose-volume histogram (DVH) was calculated for all patients.[17]

Scanning of CT images for both treatment planning and irradiation of proton beam were done during the exhalation phase using a Respiration-Gated Irradiation System (ReGIS). Our ReGIS during this study period was composed in the following manner: strain gauge, which converts tension of the abdominal wall into electrical respiratory signal, was put on the abdominal skin of the patient; gating signal triggering CT scanning or proton beam was generated during the exhalation phase.

Treatment

The fractionation and dosage in this study were based on the results of a retrospective study at the University of Tsukuba. A total dose ranging from 50 Gy$_E$ in 10 fractions to 87.5 Gy$_E$ in 30 fractions (median, 72 Gy$_E$ in 16 fractions) was administered without serious acute and late adverse events. All patients received PRT to a total dose of 76 Gy$_E$ for 5 weeks in 3.8-Gy$_E$ once-daily fractions, four fractions in a week using 150 to 190 MV proton beam. Relative biologic effectiveness of our proton beam was defined as 1.1. No concomitant treatment (eg, TACE, local ablation, systemic chemotherapy) was allowed during and after the PRT, unless a treatment failure was detected. Verification of patient set-up was done in each fraction using a digital radiography subtraction system. In this system, fluoroscopic images obtained at daily set-up were subtracted by the original image that was taken at the time of treatment planning. Position of the patient couch was adjusted to overlap the diaphragm, inserted metallic markers, and bone landmarks on the original position at the end of the exhalation phase.

PRT was administered 4 days a week, mainly Monday to Thursday, and Friday was reserved for maintenance of the PRT system. Predefined adverse reaction of PRT was dermatitis, pneumonitis, hepatic insufficiency, and gastrointestinal ulcer and/or bleeding. If one of these reactions of grade 3 or higher, or unexpected reactions of grade 4 or higher were observed in three patients, further accrual of patients was defined to be stopped. No further PRT was allowed when grade 4 hematologic toxicity or any of the toxicities of grade 3 or higher were observed at the digestive tract or lung. PRT was delayed up to 2 weeks until recovery when an acute nonhematologic toxicity of grade 3 or higher, other than that described above, was observed. However, when only an elevation of liver enzymes was observed without manifestation of clinically significant signs and symptoms, PRT was allowed to be continued according to the physician's judgment.

Outcomes

It has been reported that the tumor, although achieving a complete response, persisted over a long period, ranging from 3 weeks to 12 + months after the completion of PRT.[18] Therefore, a local progression-free survival rate at 4 weeks after the end of PRT was adopted as the primary end point of this study, where an event was defined as progression of the primary tumor with size increase of more than 25%, in order to facilitate an interim analysis as described in the Statistical Design section below. Assessment of primary tumor response using CT and/or MRI was performed 4 weeks after the completion of PRT. Overall survival and disease-free survival rates were also evaluated as secondary end points. Death of any cause was defined as an event in calculation of overall survival, whereas tumor recurrences at any sites or patient deaths were defined as events for disease-free survival. Adverse events were reviewed weekly during the PRT by means of physical examination, CBC, liver function test, and the other biochemical profiles as indicated. The severity of adverse events was assessed using the National Cancer Institute Common Toxicity Criteria (NCI-CTC) version 2.0. After completion of PRT, reviews monitoring disease status, including CT and/or MRI examinations and long-term toxicity were done at a minimum frequency of once every 3 months.

Statistical Design

The null hypothesis of a true local progression-free rate of 50% or lower was based on average results of photon radiotherapy reported from Japan, in which each study accumulated approximately 20 patients.[11,12] This was tested against the alternative hypothesis of a true rate of 80% or higher with an α level of 5% and a power of 80%, which required 30 patients according to the method by Makuch and Simon.[19] If fewer than five patients experienced local progression-free status within 4 weeks postirradiation at the end of first nine enrollments, the trial would be stopped. Otherwise, if more than 24 patients remained locally progression-free among the total of 30 patients, this would be sufficient to reject the null hypothesis and conclude that PRT warrants further study. Time-to-event analyses were done using Kaplan-Meier estimates, and 95% CIs were calculated. The difference of time-to-event curve was evaluated with the log-rank test. Multivariate analyses were performed with Cox's proportional hazards model.

RESULTS

Patients

Thirty patients were enrolled between May 1999 and February 2003. Patient characteristics at the start of PRT are

Table 1. Characteristics of 30 Enrolled Patients

Characteristic	No.	%
Age, years		
Median	70	
Range	48-87	
Sex		
Male	20	67
Female	10	33
ECOG performance status		
0-1	29	97
2	1	3
Clinical stage (2)		
I	9	30
II	19	63
III	2	7
Positive viral markers		
Hepatitis B virus	3	10
Hepatitis C virus	26	87
Both	1	3
Child-Pugh classification		
A	20	67
B	10	33
C	0	0
Pretreatment indocyanine green clearance at 15 minutes, %		
< 15	0	0
15-40	21	70
40-50	5	17
> 50	4	13
Tumor size, mm		
Median	45	
Range	25-82	
20-50	19*	63
> 50	11	37
Macroscopic vascular invasion		
Yes	12	40
No	18	60
Morphology of primary tumor		
Single nodular	26	87
Multinodular, aggregating	1	3
Diffuse	2	7
Portal vein tumor thrombosis	1*	3
Serum alpha-fetoprotein level, ng/mL		
< 300	21	70
≥ 300	9	30
Histology		
Well-differentiated	10	33
Moderately differentiated	14†	47
Poorly differentiated	2	7
Differentiation not specified	3	10
Negative (radiologic diagnosis only)	1	3
Prior treatment		
No	13	43
Recurrence	6	20
Local ablation/TACE	11	37

Abbreviations: ECOG, Eastern Cooperative Oncology Group; TACE, transarterial chemoembolization.
*Includes one patient whose gross target volume was tumor thrombosis at the posterior branch of right portal vein as a result of postsurgical recurrence.
†Includes two patients with histological diagnoses that were defined in previous surgery.

listed in Table 1. All patients had underlying liver cirrhosis with an initial ICG R15 value of ≥ 15%. Thirteen patients received PRT as a first treatment for their HCC. Six patients had postsurgical recurrences, and 11 received unsuccessful local ablation and/or TACE to the targeted tumor before PRT. Histologic confirmation was not obtained in one patient who had tumor with typical radiographic features compatible with HCC. Vascular invasion was diagnosed as positive in 12 patients. Three patients had HCC of ≤ 3 cm in diameter; however, they were not considered as candidates for local ablation therapy because of tumor locations that were in close proximity to the great vessels or the lung.

Adverse Events

All patients completed the treatment plan and received 76 Gy_E in 20 fractions of PRT with a median duration of 35 days (range, 30 to 64 days). Prolongation of overall treatment time of more than 1 week occurred in four patients: three were due to availability of the proton beam, and one because of fever associated with grade 3 elevation of total bilirubin that spontaneously resolved within 1 week. Adverse events within 90 days from commencement of PRT are listed in Table 2. Decrease of blood cell count was observed most frequently. A total of 10 patients experienced transient grade 3 leukopenia and/or thrombocytopenia without infection or bleeding necessitating treatment. Of note, eight of them already had leuko- and/or thrombocytopenia, which could be ascribable to portal hypertension, before commencement of PRT corresponding to grade 2 in terms of the NCI-CTC criteria. Because none of the five patients experiencing grade 3 elevation of transaminases showed clinical manifestation of hepatic insufficiency and maintained good performance status, PRT was not discontinued. Nevertheless, these events spontaneously resolved within 1 to 2 weeks.

Development of hepatic insufficiency within 6 months after completion of PRT was defined as proton-inducing hepatic insufficiency (PHI), and this was observed in eight patients. Causal relationship between PHI and several factors are described separately below. One patient developed transient skin erosion at 4 months that spontaneously resolved within 2 months. Another patient developed painful subcutaneous fibrosis at 6 months that required nonsteroi-

dal analgesics for approximately 12 months thereafter. Both of these skin changes developed at the area receiving ≥ 90% of the prescribed dose because the targeted tumors were located at the surface of the liver adjacent to the skin. However, they remained free from refractory ulcer, bleeding, or rib fracture.

There were no observations made of gastrointestinal or pulmonary toxicity of grade 2 or greater in all patients. In addition, after percutaneous insertion of metallic markers, no serious adverse events, including bleeding or tumor seeding along the needle tracts, were observed.

Tumor Control and Survival

At the time of analysis on November 2003, 12 patients had already died because of intrahepatic recurrence of HCC in seven, distant metastasis in two, and hepatic insufficiency without recurrence in three. Eleven of these 12 patients had been free from local progression until death; the durations ranged from 6 to 41 months (median, 8 months). One patient who had a single nodular tumor of 4.2 cm in diameter experienced local recurrence at 5 months and subsequently died of multifocal intrahepatic HCC recurrence. Otherwise, 18 patients were alive at 16 to 54 months (median, 31 months) without local progression. A total of 24 patients achieved complete disappearance of the primary tumor at 5 to 20 months (median, 8 months) post-PRT. Five had residual tumor mass on CT and MRI images for 3 to 35 months (median, 12 months) until the time of death (n = 4) or until last follow-up at 16 months (n = 1). As a whole, 29 of 30 enrolled patients were free from local progression until death or last follow-up, and the local progression-free rate at 2 years was 96% (95% CI, 88% to 100%). Tumor regression was associated with gradual atrophy of the surrounding noncancerous portion of the liver that initially suffered from radiation hepatitis,[20] as shown in Figure 1.

A total of 18 patients developed intrahepatic tumor recurrences that were outside of the PTV at 3 to 35 months (median, 18 months) post-PRT. Five of these occurred within the same segment of the primary tumor. Eight patients received TACE, and four received radiofrequency ablation for recurrent tumors; however, six did not receive any further treatment because of poor general condition in three and refusal in three. Five died without intrahepatic recurrence. Seven patients remained recurrence-free at 16 to 39 months (median, 35 months). Actuarial overall survival rates were 77% (95% CI, 61% to 92%), 66% (95% CI, 48% to 84%), and 62% (95% CI, 44% to 80%), and disease-free survival rates were 60% (95% CI, 42% to 78%), 38% (95% CI, 20% to 56%), and 16% (95% CI, 1% to 31%) at 1, 2, and 3 years, respectively (Fig 2).

Correlation of Survival With Prognostic Factors

Overall survival was evaluated according to 10 factors as listed in Table 3. Univariate analyses revealed that factors

Table 2. Adverse Events Within 90 Days From the Start of Proton Beam Radiotherapy

Grade	0	1	2	3	4
Leukopenia	7	2	13	8	0
Thrombocytopenia	2	6	15	7	0
Total bilirubin	20	2	7	1	0
Transaminases	4	8	13	5	0
Nausea/anorexia	23	7	0	0	0
Overall (maximum grade)	0	4	14	12	0

Mar 2, 2001, AFP 11335.5 ng/mL

20%
50%
90%
100%

Jun 11, 2001   Aug 13, 2001   Feb 7, 2002   Feb 3, 2003

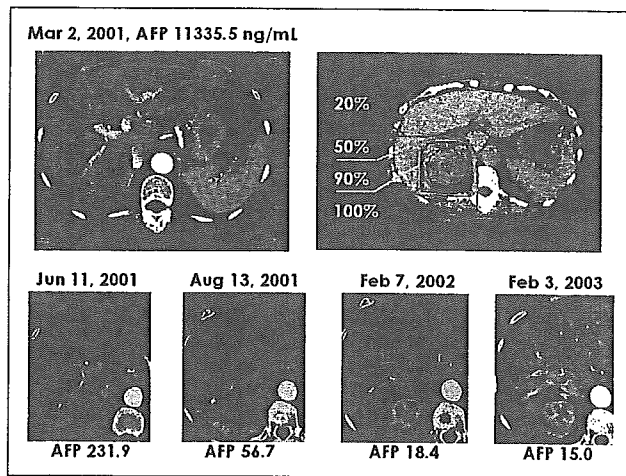AFP 231.9   AFP 56.7   AFP 18.4   AFP 15.0

Fig 1. Case presentation: 70-year-old woman who received proton radio-therapy of 76 Gy in 20 fractions for 37 days from April 2, 2001, for her tumor located at the right posterior segment of the liver (left upper panel). Dose distribution was demonstrated in the right upper panel. Two portals from posterior and right lateral directions were used.

related to functional reserve of the liver and tumor size had significant influences on overall survival ($P < .05$). Liver function was the only independent and significant prognostic factor by multivariate analysis, as presented in Table 3. When clinical stage or Child-Pugh classification was substituted for ICG R15 as a covariate for liver function, the results of multivariate analyses were unchanged (data not shown). Overall survival according to pretreatment ICG R15 is shown in Figure 3.

Estimation of the Risk of Proton-Inducing Hepatic Insufficiency by Dose-Volume Histogram Analysis

Eight patients developed PHI and presented with ascites and/or asterixis at 1 to 4 months after completion of PRT, without elevation of serum bilirubin and transaminases in the range of more than 3× the upper limit of normal. Of these, four died without evidence of intrahepatic tumor recurrence at 6 to 9 months; three died with
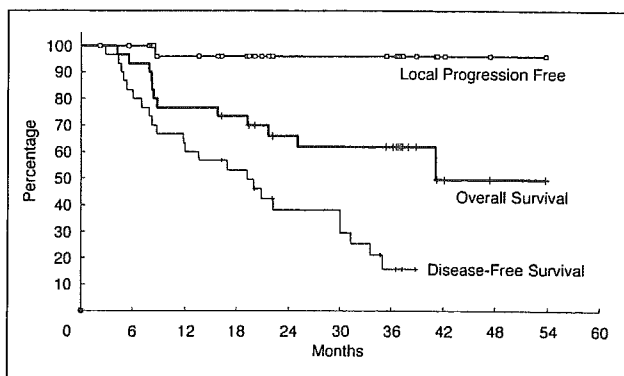

Fig 2. Kaplan-Meier estimate of local progression-free, overall, and disease-free survival rates for all 30 patients enrolled.

recurrences of HCC at 4, 8, and 22 months; and one was alive at 41 months without tumor recurrence. DVH for hepatic noncancerous portions (entire liver volume minus gross tumor volume) was drawn according to pretreatment ICG R15 values (Fig 4A to C). The results showed that all of the nine patients with ICG R15 less than 20% were free from PHI and alive at 14 to 54 months. Three of the four patients with pretreatment ICG R15 ≥ 50% experienced fatal PHI without evidence of HCC recurrence, and another patient died of PHI with intrahepatic and systemic dissemination of HCC at 4 months. Among patients whose ICG R15 values ranged from 20% to 50%, all of the four patients whose percentage of hepatic noncancerous portions receiving ≥ 30 Gy_E (V_{30}%) exceeded 25% developed PHI. On the other hand, none of the patients whose V_{30}% was less than 25% experienced PHI, as shown in Figure 4B ($P = .044$, Mann-Whitney U test). Three-year overall survival for patients with either the V_{30}% ≥ 25% or ICG R15 ≥ 50% (n = 9) was 22% (95% CI, 0% to 50%), whereas it was 79% (95% CI, 60% to 98%) for the remaining 21 patients with favorable risk ($P = .001$).

DISCUSSION

The principal advantage of PRT lies in its possibility of aggressive dose escalation without prolongation of treatment duration in order to improve local control rate. The liver will be the most appropriate organ for this approach because it has a unique characteristic of developing compensatory hypertrophy when a part of this organ suffers from permanent damage. This study showed that the local control rate of PRT alone for patients with advanced HCC was consistent, as previously reported.[14] Slow regression of tumor volumes associated with gradual atrophy of surrounding noncancerous liver tissue was also in agreement with a previous report.[20] No serious gastrointestinal toxicity occurred, with careful patient selection performed in order to exclude these structures from PTV receiving high PRT dose. Eligibility criteria as to blood cell count in this study were eased up considerably in order to test the safety of PRT for patients with cirrhosis associated with portal hypertension. Nevertheless, no patients experienced serious sequelae relating to leukopenia or thrombocytopenia, which were the most frequently observed adverse events during PRT. All patients were able to complete their PRT basically in an outpatient clinic. Therefore we submit that the safety, accuracy, and efficacy of PRT administering 76 Gy_E/5 weeks using our newly installed Proton Therapy System and ReGIS for selected patients with advanced HCC has been confirmed.

Multivariate analysis suggested that the the functional reserve of the liver had significant influence on overall survival. Recent prospective series of untreated patients with

Table 3. Factors Related to Overall Survival

Factor	No. of Patients	Overall Survival at 2 Years (%)	Univariate P	Multivariate P	Hazard Ratio	95% CI
Age, years			.263	.665	1.54	0.22 to 10.75
< 70	15	59				
≥ 70	15	71				
Sex			.829	.732	1.44	0.18 to 11.65
Male	20	67				
Female	10	60				
Tumor size, mm			.045	.159	0.34	0.08 to 1.52
20 to 50	19	71				
> 50	11	44				
Pretreatment ICG R15			.006	.026	0.19	0.05 to 0.82
≤ 40%	21	80				
> 40%	9	30				
Clinical stage			< .001			
I	9	73				
II	19	68				
III	2	0				
Child-Pugh classification			.006			
A	20	78				
B	10	38				
Vascular invasion			.930	.650	1.44	0.30 to 7.03
Yes	12	67				
No	18	66				
Serum AFP level, ng/mL			.313	.061	0.20	0.04 to 1.07
< 300	21	67				
≥ 300	9	60				
V_{30}%			.213	.141	0.25	0.04 to 1.58
≤ 25%	24	65				
> 25%	6	40				
Prior treatment			.455	.091	3.63	0.82 to 16.18
No	13	69				
Recurrence	17	60				

Abbreviations: ICG R15, percentage of indocyanine green clearance at 15 minutes; AFP, alpha-fetoprotein; V_{30}%, percentage of hepatic noncancerous portion receiving ≥ 30 cobalt gray equivalent.

advanced HCC and underlying cirrhosis showed that overall survival rate at 3 years ranged from 13% to 38%, and rarely exceeded 50% even for those with most favorable prognostic factors.[1] In this study, actuarial overall survival
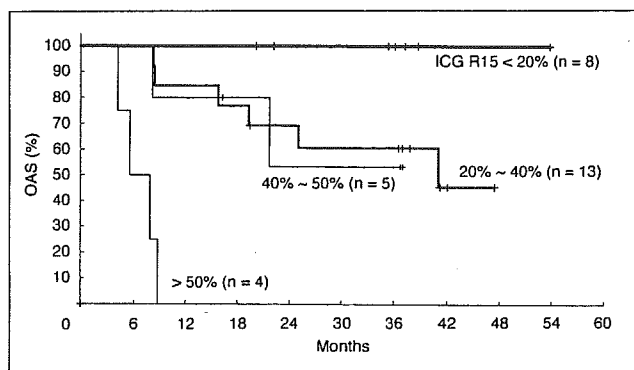

Fig 3. Overall survival (OAS) rates according to pretreatment indocyanine green clearance at 15 minutes (ICG R15).

rate at 3 years for all 30 patients including those who had HCC with vascular invasion and/or severe cirrhosis was 62%. Furthermore, 21 patients with initial ICG R15 of ≤ 50% and V_{30}% of ≤ 25% achieved 79% of overall survival rate at 3 years. All of the eight patients with favorable liver functional reserve (ICG R15, 15% to 20%) were alive at 20 to 54 months as shown in Figure 3. This suggests that adequate local control with PRT provides survival benefit for selected patients with HCC and moderate cirrhosis. On the other hand, prognoses of aggressive PRT were disappointing for patients, with poor functional liver reserve showing an ICG R15 of 50% or worse, and, therefore, indication of PRT for such patients was thought to be extremely limited.

A part of noncancerous liver suffering from PRT-inducing hepatitis gradually developed dense fibrosis and resulted in almost complete atrophy,[20] whereas the absorbed dose in a large proportion of the remaining liver was 0 Gy_E, as shown in Figures 1 and 4. This change is similar to